SANDIA REPORT

SAND89—0592 • UC—814
Unlimited Release
Printed March 1991

A Constitutive Model for Jointed Rock Mass With Two Intersecting Sets of Joints

E. P. Chen

Prepared by
Sandia National Laboratories
Albuquerque, New Mexico 87185 and Livermore, California 94550
for the United States Department of Energy
under Contract DE-AC04-76DP00789

DISCLAIMER

Issued by Sandia National Laboratories, operated for the United States Department of Energy by Sandia Corporation.

Printed in the United States of America. This report has been reproduced directly from the best available copy.

Available to DOE and DOE contractors from
Office of Scientific and Technical Information
PO Box 62
Oak Ridge, TN 37831

Prices available from (615) 576-8401, FTS 626-8401

Available to the public from
National Technical Information Service
US Department of Commerce
5285 Port Royal Rd
Springfield, VA 22161

NTIS price codes
Printed copy: A03
Microfiche copy: A01

SAND--89-0592

DE91 010651

SAND89-0592
Unlimited Release
Printed March 1991

A Constitutive Model for Jointed Rock Mass with Two Intersecting Sets of Joints

E. P. Chen
Engineering and Structural Mechanics Division 1514
Sandia National Laboratories
Albuquerque, New Mexico 87185

Abstract

A constitutive model that describes the response of a jointed rock mass under applied loads has been developed in this investigation following similar procedures used previously by the author for two orthogonal joint sets. However, the present model is more general than the orthogonal joint set model because the joint sets can intersect at arbitrary angles. The mechanical behavior of the intact rock is considered elastic while the joint closure and slip response are nonlinear in nature. By using the constitutive model, the field equations have been reduced to a fourth-order algebraic equation for the solution of stresses; this equation is given explicitly in the text. Example problems have been solved to show how the rock mass responds to loads, and the effects of joint sets intersecting at nonorthogonal angles have been investigated and presented.

This work was performed under the auspices of the U.S. Department of Energy (US DOE), Office of Civilian Radioactive Waste Management, Yucca Mountain Project, under Contract #DE-AC04-76DP00789. The (data) (analyses) for this document were gathered under Quality Assurance Level 3. WBS 1.2.4.6.1.

Contents

Figures

Page

1. Introduction

This investigation involves the development of a general two-dimensional continuum model to describe jointed rock mass. Chen (1986,1989) recently developed a model for the analysis of rock mass containing two orthogonal joint sets. Development of the orthogonal joint set model followed the general formulation of Morland (1974) and the special single joint set implementation of Morland's model by Thomas (1982). Although the orthogonal joint set model has proven useful for analyzing field-scale problems (see Costin and Chen; 1988a, 1988b), it remains restrictive in terms of the general field conditions. In this paper, the orthogonal joint set model has been extended to a more general model where the orthogonality restriction has been relaxed. Fundamental approaches remain the same for both models. However, as the general model becomes capable of treating physically more complicated problems, it becomes mathematically more complex. This complexity provides the potential to study more completely the interaction of various parameters representing the characteristics of jointed rock mass behavior. The equation governing the solution of the problem has been given, and example problems have been solved. The behavior of the rock mass predicted by the orthogonal joint set model has been compared to the general model.

This model has been developed to aid in characterizing the site of the repository at Yucca Mountain, Nevada, for the potential geologic disposal of radioactive waste. Disposal of high-level nuclear waste is currently being considered by the Yucca Mountain Project, administered by the Nevada Operations Office of the U. S. Department of Energy.

2. Constitutive Model Formulation and Solution

As has been mentioned previously, the procedure for developing the general model is the same as that given in Chen (1986,1989) for the orthogonal joint set model. The arrangement of a representative element of a jointed rock mass is shown in Figure 1. In this figure, two joint sets with joint spacings δ_1 and δ_2 are inclined against each other with an included angle θ. The joints in a given set are assumed to be regularly spaced and parallel. In the plane of the joints, the orientation of the joint sets is characterized by the angles θ_1 and θ_2 with respect to a reference Cartesian coordinate xyz system, as shown in Figure 2. The plane of the joints are in the xy-plane. Also given in Figure 2 are the in-plane normals n_1 and n_2 and the out-of-plane normals t_1 and t_2 to the sets of joints. Note that the directions z, t_1, and t_2 coincide. Following the work of Morland (1974), a continuous displacement field can be defined that represents the average response of the joints. While this displacement field cannot give the individual responses of the joints, it captures the gross responses of all joints in an average sense. Based on the continuous displacement fields for the joints, a strain partitioning equation can be written for the rock mass in which the total strain is equal to the sum of the strains of the intact rock and the joints. The constitutive behavior for the intact rock is considered elastic. For a single joint, normal closure is assumed to be nonlinear elastic and to follow the empirical behavior given by Goodman (1976):

$$T_{nn} = -A\left(\frac{u^d}{u^d_{max} - u^d}\right) \tag{1}$$

where T_{nn} and u^d, the normal stress component and the corresponding displacement across the joint, are positive in tension. The constant A is referred to as the half-closure stress and u^d_{max} is the maximum amount of closure that can be sustained by the joint (see Figure 3 for definitions of these quantities). The joint is allowed to carry tension to expedite the numerical computations. Because the allowable tension is relatively small (maximum tension carried by the joint will not exceed the magnitude of the half- closure stress even for very large opening displacements), the gain in computation speed seems to outweigh this minor physical discrepancy. The joint slip behavior is defined by a bilinear shear stress-slip displacement response, shown in Figure 4. The onset of nonlinearity is governed by the Mohr-Columb criterion as

$$|\ \tau_p\ | = C_0 - \mu T_{nn} \tag{2}$$

in which C_0 and μ are, respectively, the cohesion and the coefficient of Coulomb friction.

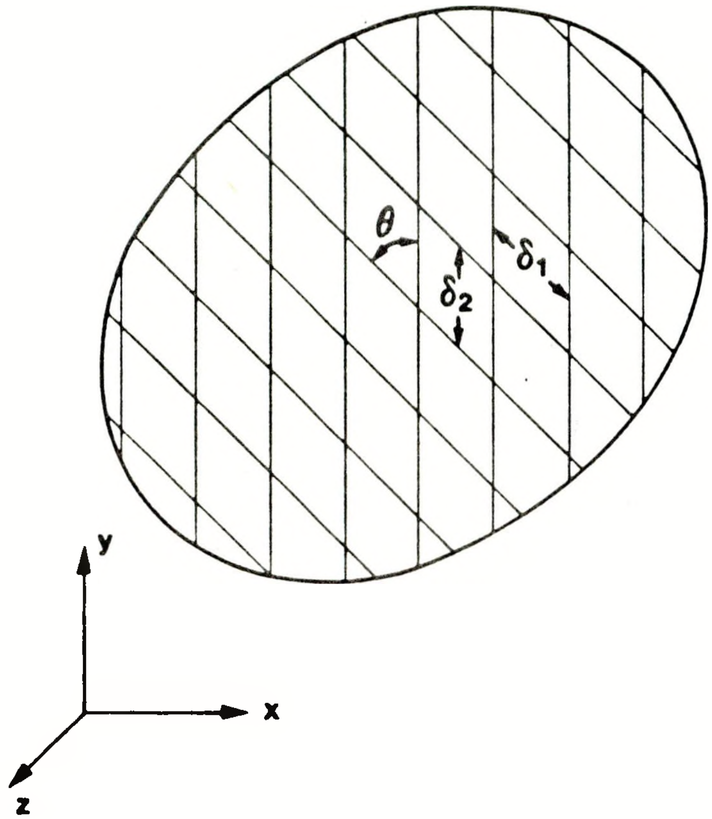

Figure 1. Geometry of Jointed Rock Mass

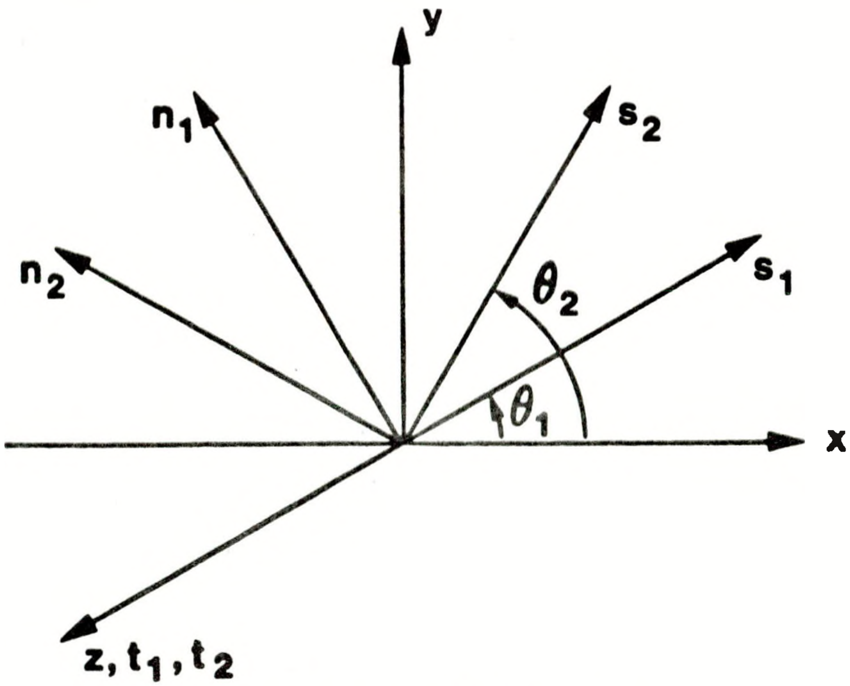

Figure 2. Joint Orientation Definitions

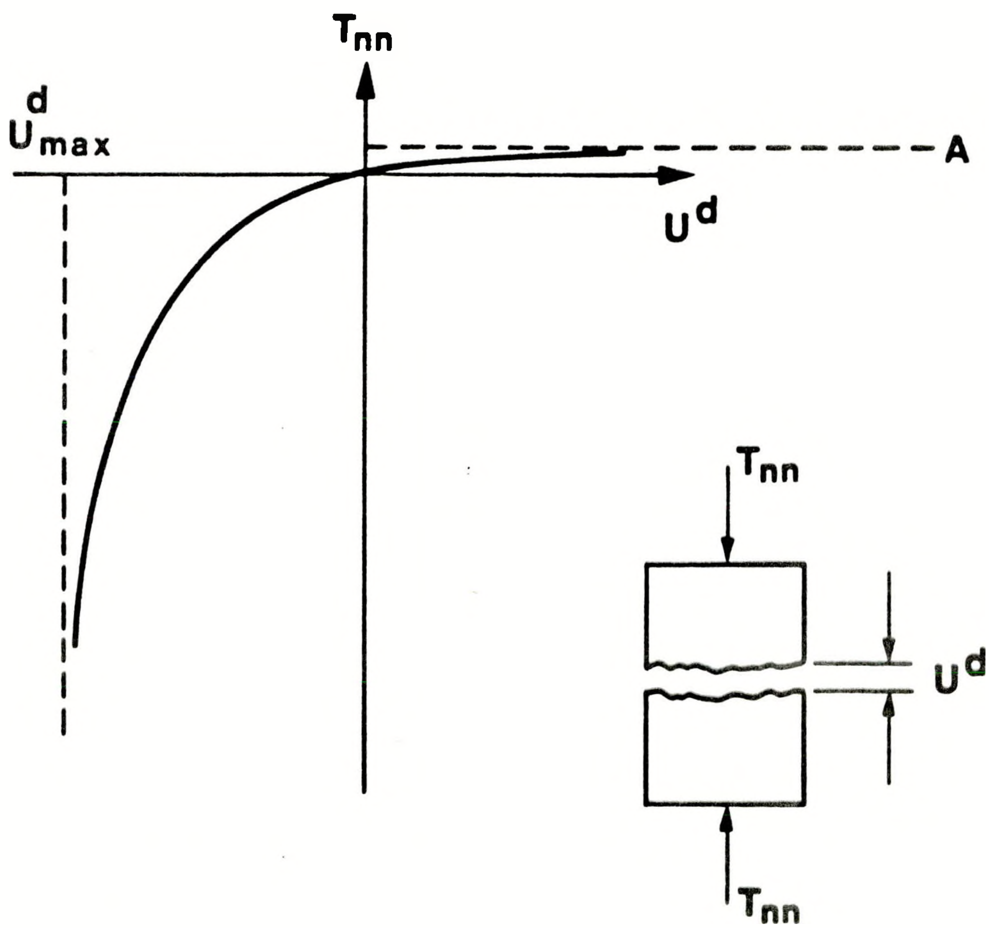

Figure 3. Nonlinear Normal Joint Closure Behavior

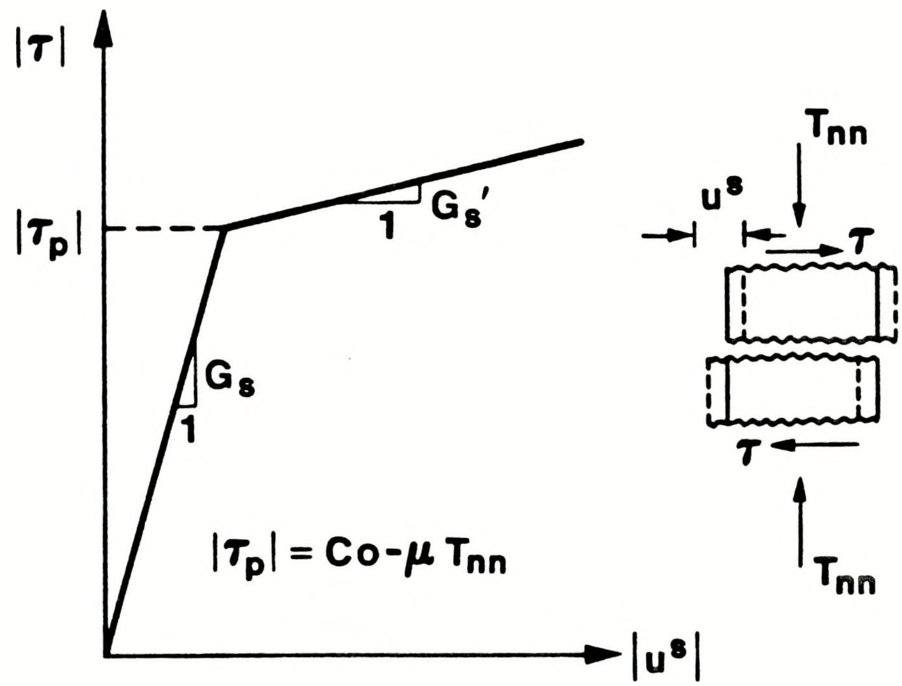

Figure 4. Nonlinear Shear Behavior of Joints

Because the problem is nonlinear in nature, incremental procedures are used to obtain solutions. The strain partitioning relationships and the above constitutive models for the intact rock and joints can be combined to establish a set of rate equations for calculating stress increments in terms of strain increments. This procedure is the same as that given by Chen (1986,1989) for orthogonal joint sets. In Chen (1986,1989), the problem was reduced to the solution of a fourth-order algebraic equation. In the present general case, it has been found that the problem can also be reduced to the solution of a fourth-order algebraic equation. However, the solution for the general case is more complicated because without orthogonality, coupling occurs between the normal and shear stress components. Moreover, the coefficients in the equation become more complex because an additional parameter, the included angle between the two joint sets, also appears.

In the remainder of this section, the algebraic expressions necessary for numerical implemention of the present model are presented. Note that the resulting fourth-order equation can be solved by the same procedure as given in Chen (1989). Let the bulk modulus and the shear modulus of the intact rock be K and G, respectively. For joint set i, i=1,2, the half-closure stress is A_i, the maximum closure is $(u^d_{max})_i$, and the slopes of the bilinear shear stress-slip displacement curve are G_{si} and G'_{si}, respectively, for the initial and the hardening part. Without going into details, the fourth-order algebraic equation to calculate the normal stress for joint set 1 at time step t+1 advancing from time step t is derived as [for detailed derivation procedure, references are made to the work of Chen (1986, 1989)]:

$$a_1 T_n^4 + a_2 T_n^3 + a_3 T_n^2 + a_4 T_n + a_5 = 0 \qquad (3)$$

in which $T_n = A_1 - T^{t+1}_{n_1 n_1}$ and the coefficients are

$$a_1 = \frac{4GS^2(1 - \alpha_6 + \alpha_5) + 2S^2\alpha_5\alpha_6\alpha_8 + \alpha_1\alpha_7}{2S^2\alpha_5(2GC + \alpha_6\alpha_8) + \alpha_3\alpha_7} \qquad (4)$$

$$a_2 = \gamma_{10} - b_1\gamma_{11}, \quad a_3 = (2G\beta_2 - \gamma_{10}\, gamma_{11})b_3 - a_1 b_2 - (b_4 - b_5 + b_6) \qquad (5)$$

$$a_4 = (b_4 - b_5 + b_6)b_3\gamma_{11} - b_2\gamma_{10}, \quad a_5 = b_2(b_4 - b_5 + b_6)\,. \qquad (6)$$

In the above equations, the following contractions have been made:

$$\alpha_1 = K + 4G/3\,, \quad \alpha_2 = K - 2G/3\,, \quad \alpha_3 = K - 2G(1/3 - cos^2\theta) \qquad (7)$$

$$\alpha_4 = K - 2G(1/3 - sin^2\theta)\,, \quad \alpha_5 = \frac{G}{\delta_2 G_{s2}}\,, \quad \alpha_6 = 1 + \frac{G}{\delta_1 G_{s1}} \qquad (8)$$

$$\alpha_7 = \alpha_5 C^2 + \alpha_6\,, \quad \alpha_8 = 2(K + G/3)\,, \quad \alpha_9 = \alpha_1\alpha_4 - \alpha_2\alpha_3 \qquad (9)$$

$$S = sin\theta cos\theta\,, \quad C = cos^2\theta - sin^2\theta\,, \quad \beta_i = -A_i(u^d_{max})_i/\delta_i\,, \quad i = 1,2 \qquad (10)$$

$$b_1 = -\frac{4GS^2(1-\alpha_6+\alpha_5) + 2S^2\alpha_5\alpha_6\alpha_8 + \alpha_1\alpha_7}{2G(4S^2\alpha_5\alpha_6+\alpha_7)} \tag{11}$$

$$b_2 = \frac{\beta_1\{2S^2\alpha_5\alpha_6(\alpha_1+\alpha_2)+\alpha_1\alpha_7\}}{4S^2\alpha_5\alpha_6+\alpha_7}, \quad b_3 = -\frac{2S^2\alpha_5(2GC+\alpha_6\alpha_8)+\alpha_3\alpha_7}{2G(4S^2\alpha_5\alpha_6+\alpha_7)} \tag{12}$$

$$b_4 = \frac{\beta_1 sin^2\theta(\alpha_1\alpha_4-\alpha_2\alpha_3)(\alpha_6-\alpha_5 C)}{2S^2\alpha_5(2GC+\alpha_6\alpha_8)+\alpha_3\alpha_7} \tag{13}$$

$$b_5 = \frac{4G\beta_1 S^2\alpha_5 C(\alpha_1+\alpha_2)sin^2\theta}{2S^2\alpha_5(2GC+\alpha_6\alpha_8)+\alpha_3\alpha_7}, \quad b_6 = \frac{4G\beta_1 S^2\{\alpha_1+2S^2\alpha_5(\alpha_1+\alpha_2)\}}{2S^2\alpha_5(2GC+\alpha_6\alpha_8)+\alpha_3\alpha_7} \tag{14}$$

$$p_1 = \frac{\alpha_4\alpha_7 - 2S^2\alpha_5(2GC-\alpha_6\alpha_8)}{2S^2\alpha_5(2GC+\alpha_6\alpha_8)+\alpha_3\alpha_7}, \quad p_3 = \frac{2G(1+\alpha_5)}{2S^2\alpha_5(2GC+\alpha_6\alpha_8)+\alpha_3\alpha_7} \tag{15}$$

$$p_2 = \frac{\beta_1\{\alpha_7(\alpha_1\alpha_4-\alpha_2\alpha_3) - 4\alpha_5 GCS^2(\alpha_1+\alpha_2)\}}{2S^2\alpha_5(2GC+\alpha_6\alpha_8)+\alpha_3\alpha_7} \tag{16}$$

$$p_4 = \frac{\beta_1\{2G(\alpha_1+2S^2\alpha_5(\alpha_1+\alpha_2)) - \alpha_5 C(\alpha_1\alpha_4-\alpha_2\alpha_3)\}}{2S^2\alpha_5(2GC+\alpha_6\alpha_8)+\alpha_3\alpha_7} \tag{17}$$

$$\gamma_0 = (\alpha_4-\alpha_2 C)\Delta\epsilon_{n_1n_1} - (\alpha_3+\alpha_2 C)\Delta\epsilon_{s_1s_1} - \alpha_2 C\Delta\epsilon_{t_1t_1} \tag{18}$$

$$\gamma_1 = \alpha_1 S\Delta\epsilon_{n_1n_1} + \alpha_2 S(\Delta\epsilon_{s_1s_1}+\Delta\epsilon_{t_1t_1}) - \alpha_3\Delta\epsilon_{n_1s_1} \tag{19}$$

$$\gamma_2 = \alpha_1 S\Delta\epsilon_{s_1s_1} + \alpha_2 S(\Delta\epsilon_{n_1n_1}+\Delta\epsilon_{t_1t_1}) - \alpha_4\Delta\epsilon_{n_1s_1} \tag{20}$$

$$\gamma_3 = -\frac{2G\{2S\alpha_5 C(\gamma_1+\gamma_2)+\alpha_7\gamma_0\}}{2S^2\alpha_5(2GC+\alpha_6\alpha_8)+\alpha_3\alpha_7} \tag{21}$$

$$\gamma_4 = -\frac{2G\{S\alpha_5(2S(\gamma_1+\gamma_2)+C\gamma_0)+\gamma_1\}}{2S^2\alpha_5(2GC+\alpha_6\alpha_8)+\alpha_3\alpha_7} \tag{22}$$

$$\gamma_5 = -\{2G\Delta\epsilon_{n_1s_1} + \alpha_5 CS\gamma_3 - (\alpha_6+\alpha_5 C^2)\gamma_4\}/S \tag{23}$$

$$\gamma_6 = \gamma_5 + \frac{2G\beta_2}{A_2 - T^t_{n_2n_2}} - \frac{T^t_{n_1n_1}}{b_3} - \frac{b_2}{b_3(A_1 - T^t_{n_1n_1})} \tag{24}$$

$$\gamma_7 = \gamma_3 - p_1 T^t_{n_1n_1} + T^t_{s_1s_1} - \frac{p_2}{A_1 - T^t_{n_1n_1}} \tag{25}$$

$$\gamma_8 = \gamma_4 + Sp_3 T^t_{n_1n_1} + T^t_{n_1s_1} + \frac{Sp_4}{A_1 - T^t_{n_1n_1}} \tag{26}$$

$$\gamma_9 = \gamma_7 sin^2\theta - 2S\gamma_8, \quad \gamma_{10} = A_2 - \gamma_9 - \frac{b_1 A_1}{b_3}, \quad \gamma_{11} = \gamma_6 + \frac{A_1}{b_3}. \tag{27}$$

Because the strain increments $\Delta\epsilon_{ij}$ and the stresses at the beginning of the load step T^t_{ij} are known, $T^{t+1}_{n_1n_1}$ can be obtained from Equation (3). The other stress components associated with joint set 1 can be found from

$$T^{t+1}_{s_1s_1} = p_1 T^{t+1}_{n_1n_1} + \gamma_7 + \frac{p_2}{A_1 - T^{t+1}_{n_1n_1}} \tag{28}$$

$$T^{t+1}_{n_1 s_1} = Sp_3 T^{t+1}_{n_1 n_1} + \gamma_k + \frac{Sp_4}{A_1 - T^{t+1}_{n_1 n_1}} \tag{29}$$

$$T^{t+1}_{t_1 t_1} = T^{t}_{t_1 t_1} + \Delta T_{t_1 t_1} \tag{30}$$

where the stress increment is given by

$$\Delta T_{t_1 t_1} = \frac{6KG}{\alpha_8} \Delta \epsilon_{t_1 t_1} + \frac{\alpha_2}{\alpha_8} (\Delta T_{n_1 n_1} + \Delta T_{s_1 s_1}) \, . \tag{31}$$

Stress components in the Cartesian coordinate xyz system and in the second joint set $n_2 s_2 t_2$ reference frame can easily be determined from the above stresses through the stress transformation equations. There remains the question of determining the shear stress when the stress level exceeds the onset of nonlinearity as governed by the Coulomb criterion. When this happens, the shear stress increment is calculated from the strain partitioning equation where an analytical expression can be derived. In this manner, it is ensured that the strain partitioning equation is satisfied and that the calculated shear stress and slip displacement follow the material property curve. Again, the solution procedures are similar to those for the orthogonal joint sets model in Chen (1986.1989). A driver program has been written for the constitutive model, based on the above equations. This program calculates stress increments when strain increments are given and will be used to solve example problems to demonstrate some of the interesting features of the model.

3. Example Problems

Several example problems are solved here to demonstrate the model. The following rock properties, taken from the work of Thomas (1982), are used in all examples:

Intact Rock

K = 4.59 GPa, G = 2.76 GPa

Joint Properties

A_n = 6.89 MPa, $(u^d_{max})_n$ = -0.00762 cm

$(G_s)_n$ = 0.27 GPa/cm, $(G'_s)_n$ = 2.71 MPa/cm

μ_n = 0.7, $(C_0)_n$ = 1.72 MPa, δ_n = 1.27 cm

For convenience, both joint sets are assumed to have the same properties. The geometry of the example problems is that in Figure 5. An infinite rock mass is to be strained in the Cartesian coordinate xy-plane. One joint set has a fixed horizontal direction while the direction of the other joint set varies depending on the parameter θ. Initial stress states can also be imposed on the rock mass.

In the first example, the rock mass is loaded by uniaxial compression along the y-direction. Boundary conditions are applied such that the value for ϵ_y is varied linearly from 0.0 to -0.005 for the time history of the problem. The rock is constrained such that all other strain components (ϵ_x , ϵ_z , ϵ_{xy}) are zero during the entire loading process. An initial stress state of $\sigma_x = \sigma_y = \sigma_z$ = -1.38 MPa and τ_{xy} = 0.0 is assumed to prevail in the rock mass. Results have been obtained for θ = 30°, 60°, and 90°. The effect of the angle θ can be seen in a plot of the variation of the normal stress on the joint against the applied strain for joint sets 1 and 2 (Figures 6 and 7). From Figure 6 it is seen that the magnitude of the normal stress increases as angle θ increases. This is because, as θ increases, more load is shifted from the second joint set to the horizontal first joint set simply from the geometric configuration. For the same reason, the magnitude of the normal stress on joint set 2 should decrease with respect to increasing angle θ. This is the result shown in Figure 7. Note that the stress state in the coordinate xy-plane is the same as that for the first joint set because of the geometry selected for the example problems.

The second example involves the pure shear loading on the rock mass. The shear strain ϵ_{xy} is increased linearly from 0 to 0.01 over the time history of the problem while

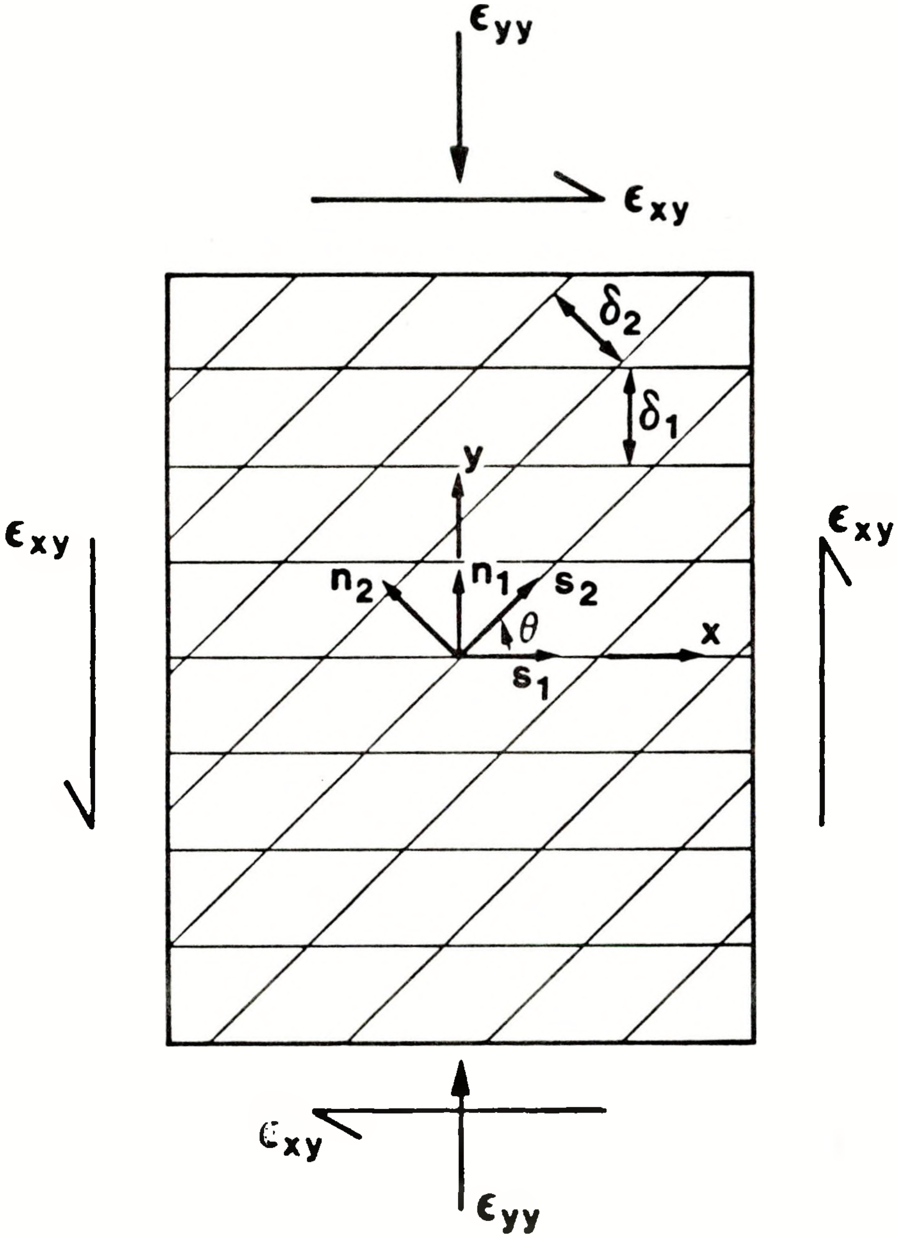

Figure 5. Example Problem Geometry

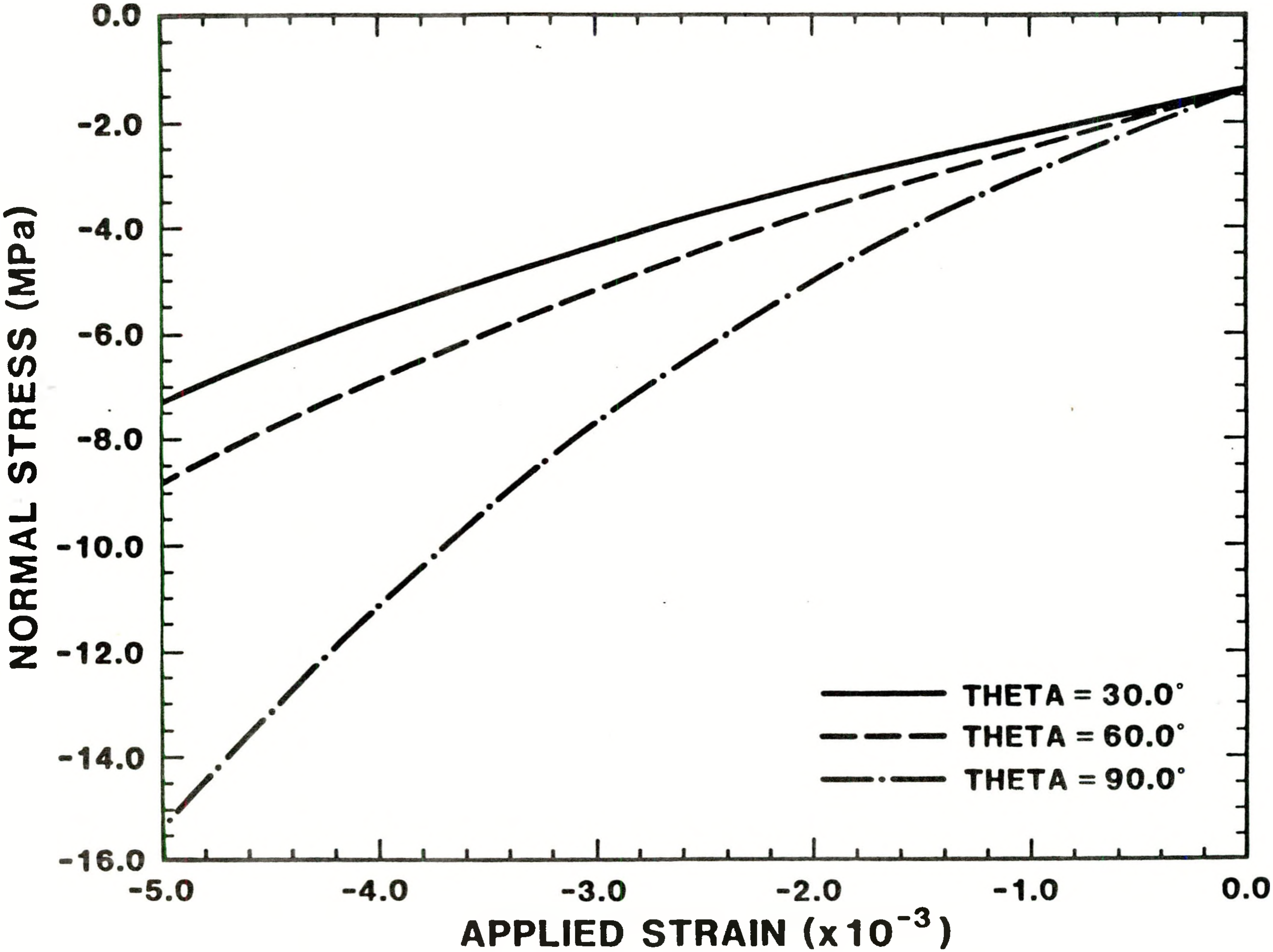

Figure 6. Stress-Strain Behavior for Joint Set 1, Example 1

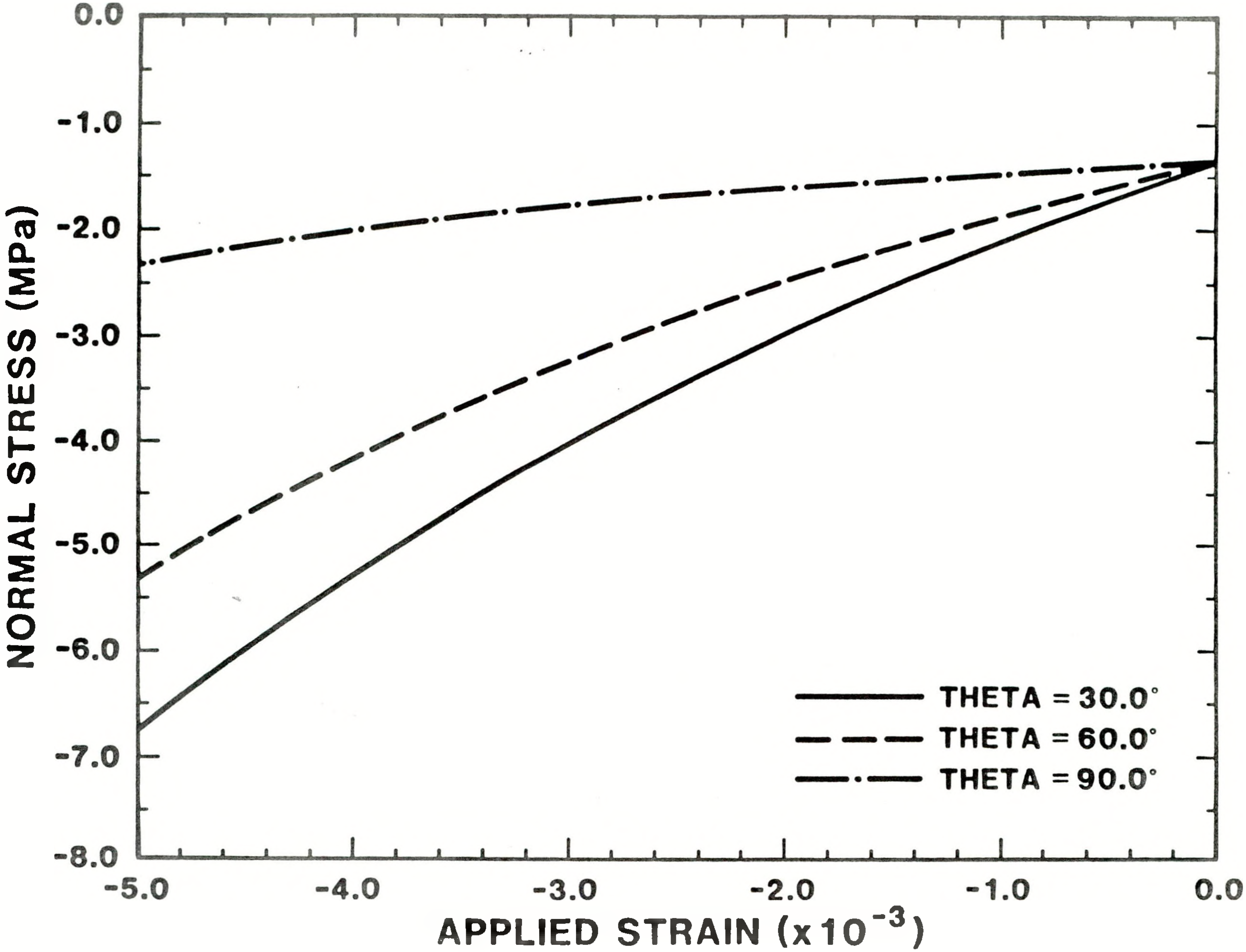

Figure 7. Stress-Strain Behavior for Joint Set 2, Example 1

all the normal strains are constrained to be zero throughout the shearing process. An initial stress state of $\sigma_x = \sigma_z$ = -1.38 MPa and σ_y = -3.45 MPa is imposed on the system. Again, the results for θ equals 30°, 60° and 90° have been calculated. Figure 8 shows the variations of the shear stress as a function of the applied shear strain for the first (horizontal) joint set. The curves are initially linear up to some applied strain level and then begin to deviate from linearity. The trend indicates that shear stress increases as the angle θ increases. The shear stress versus applied shear strain plots for the second joint set are shown in Figure 9. Because of the imposed initial stress state, the initial shear stresses for joint sets oriented at θ equal to 30° and 60° are nonzero. The magnitudes of these initial shear stresses can be calculated from a simple Mohr's circle analysis. The bilinear behaviors of the curves are similar to those for the first joint set. However, with repect to angle θ, no obvious trend for the shear stresses is observed. All curves in Figures 8 and 9 exhibit nonlinear behavior. However, in some cases, the observed nonlinearity is due to the interaction of the joints rather than the occurrence of slip nonlinearity. For the first joint set, the shear stress versus joint slip curves are plotted in Figure 10. For θ equal to 30° and 60°, slip nonlinearities have occurred. For θ equal to 90°, the shear-slip curve remains linear. The opposite is true for joint set 2, as shown in Figure 11. The complex behaviors observed in these figures are the results of the interplays among the imposed initial stress state, the applied shear strain, and the interactions between the two joint sets.

Another way to comprehend the complexities is to examine the loading paths for the two joint sets under the applied shear strain. For θ equal to 30°, plots of the shear stress magnitude versus normal stress magnitude are given in Figure 12. The solid curve in Figure 12 represents the Mohr-Coulomb criterion in the stress space. For the first joint set, because of its horizontal orientation, its initial state at point A consists of a normal stress value of 3.45 MPa and zero shear stress. The initial state at A' of the second joint set has both nonzero normal and shear stresses resulting from its 30° orientation. Between points A and B and points A' and B', which correspond to the increase in shear strain from zero, the shear stress for joint set 1 increases while the normal stress decreases. This decrease in normal stress for joint set 1 is due to the interaction between the joint sets because the second joint set takes on more normal stress and less shear stress. The onset of slip nonlinearity for the first joint set occurs at point B and the loading path from B to the end of the applied strain point C follows closely the Mohr-Coulomb criterion. The small deviation is due to the shear hardening as shown in Figure 4. For the second joint set, the stress path reverses its course from B' to C' as a result of the nonlinearity of joint set 1. However, it is clearly seen that the combination of the applied stresses on the second joint set has been below the Mohr-Coulomb criterion throughout the loading process and, consequently, no slip for the second joint set has occurred. Loading path plots for θ equal to 60° and 90° are shown, respectively, in Figures 13 and 14. The

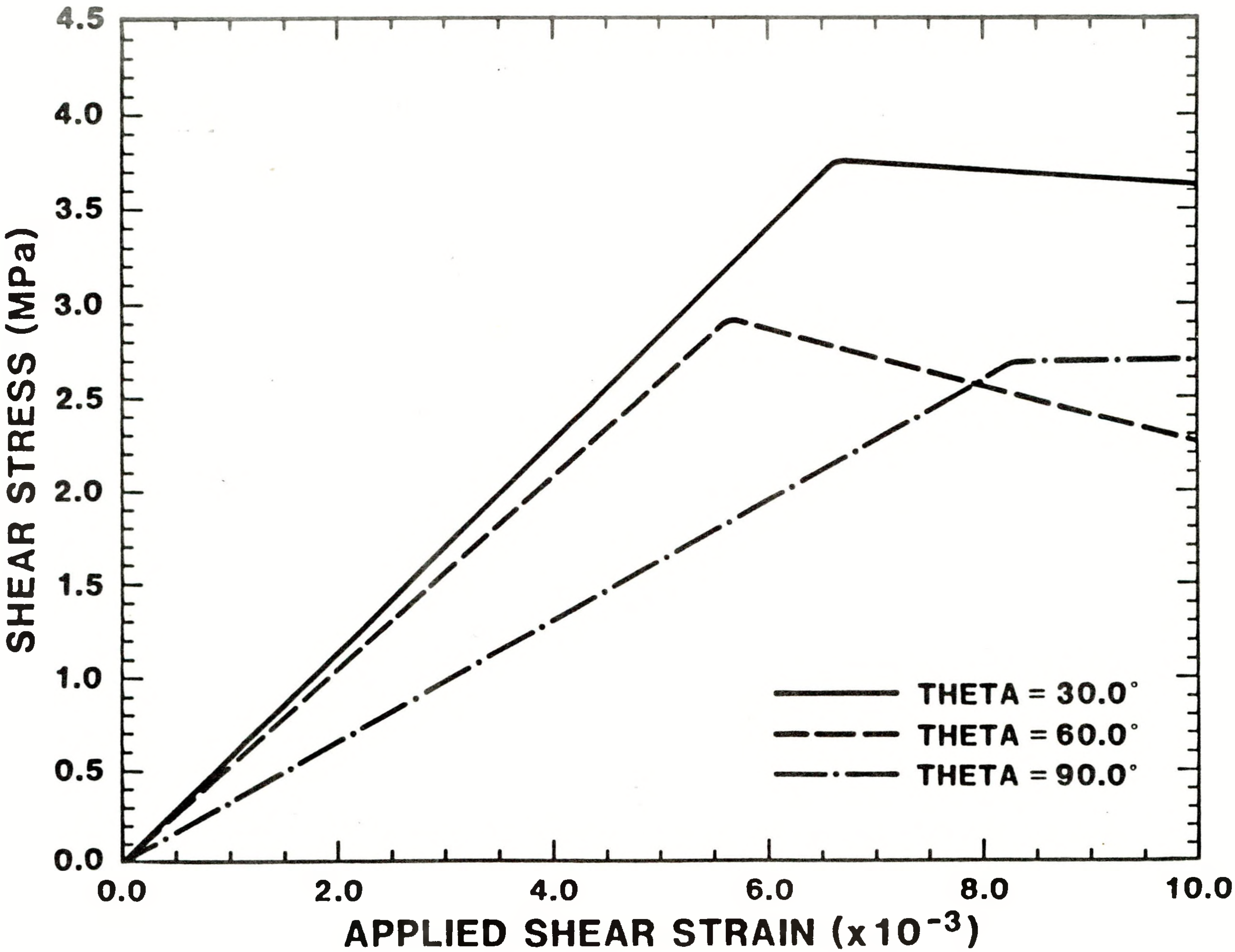

Figure 8. Stress-Strain Behavior for Joint Set 1, Example 2

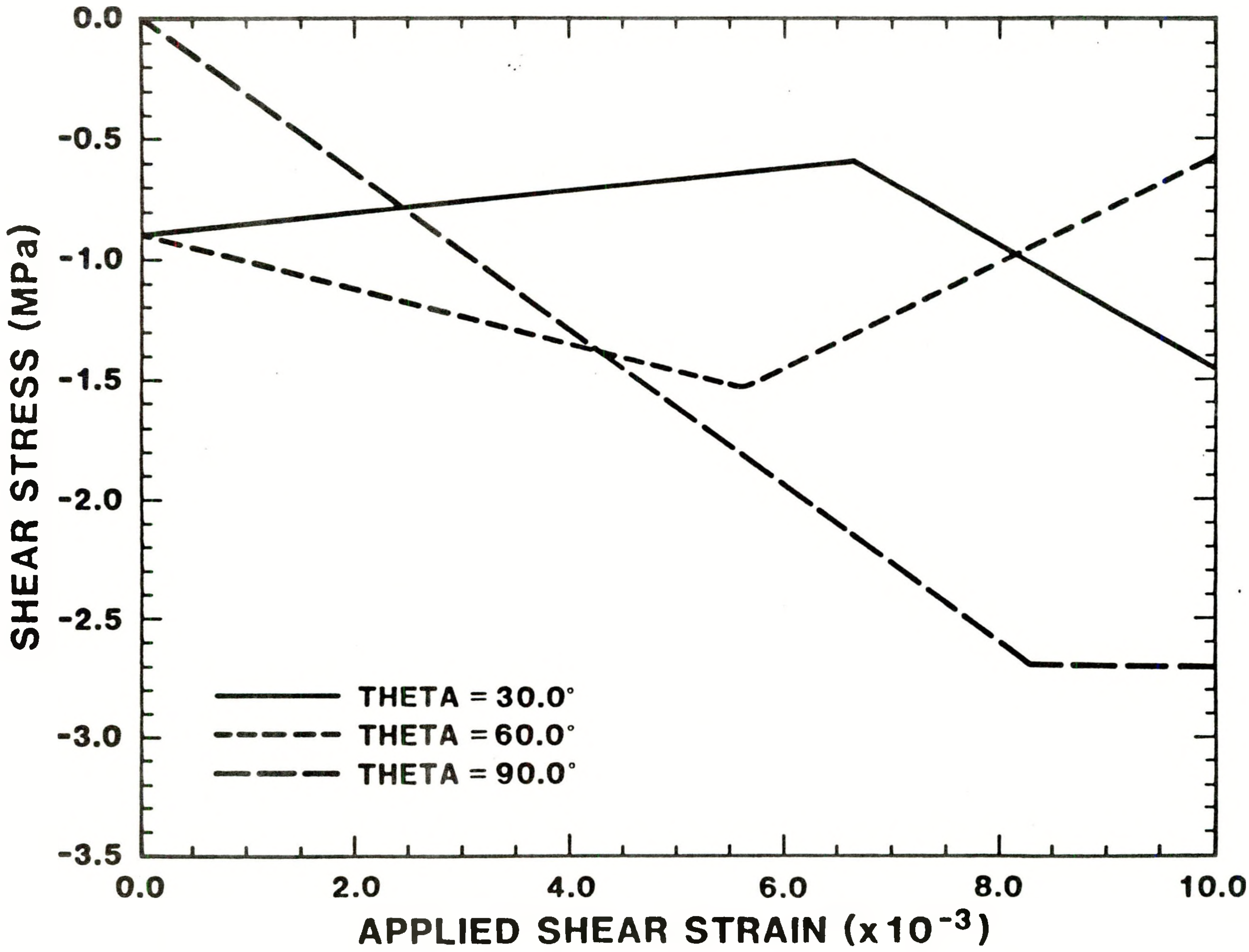

Figure 9. Stress-Strain Behavior for Joint Set 2, Example 2

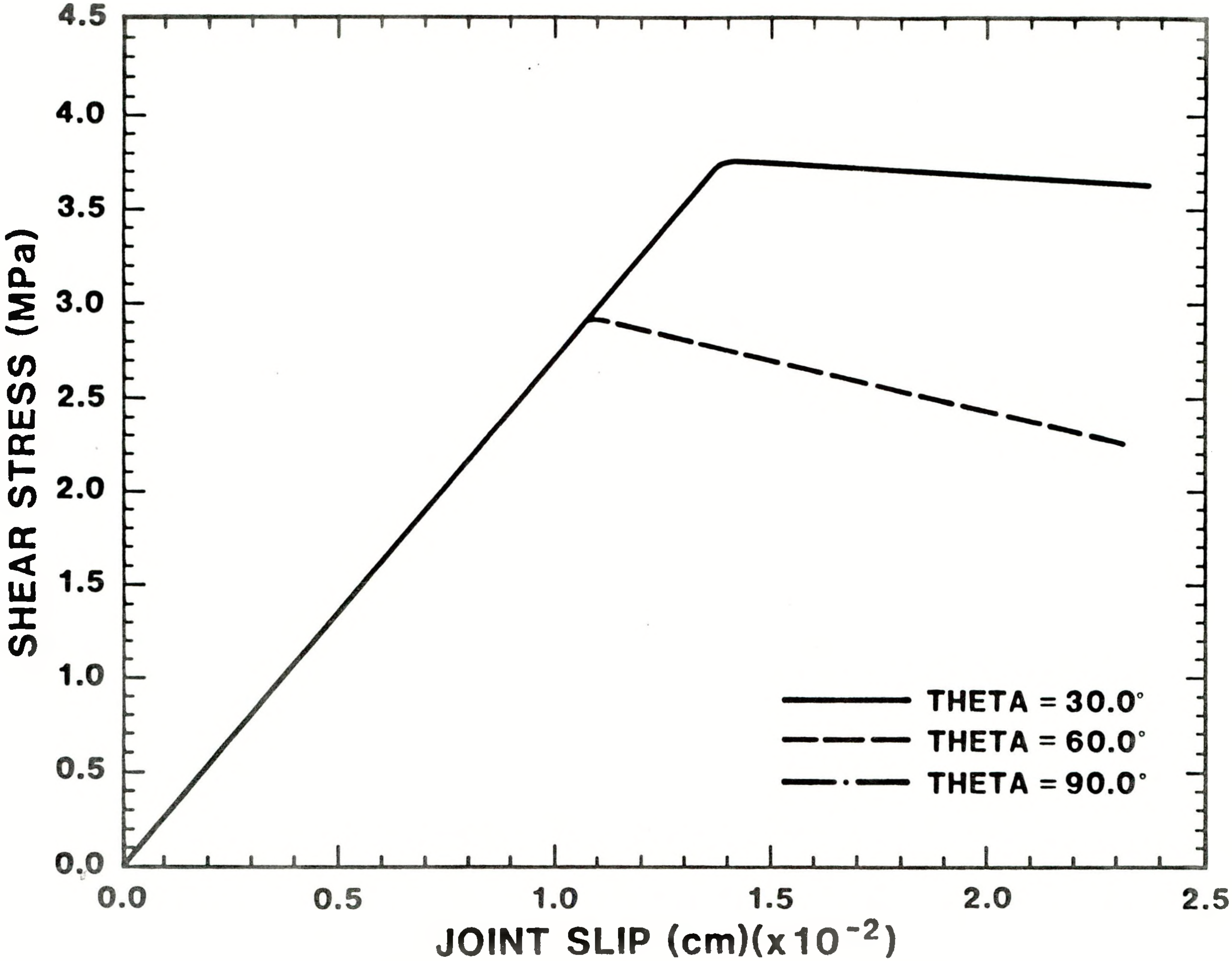

Figure 10. Stress-Slip Behavior for Joint Set 1, Example 2

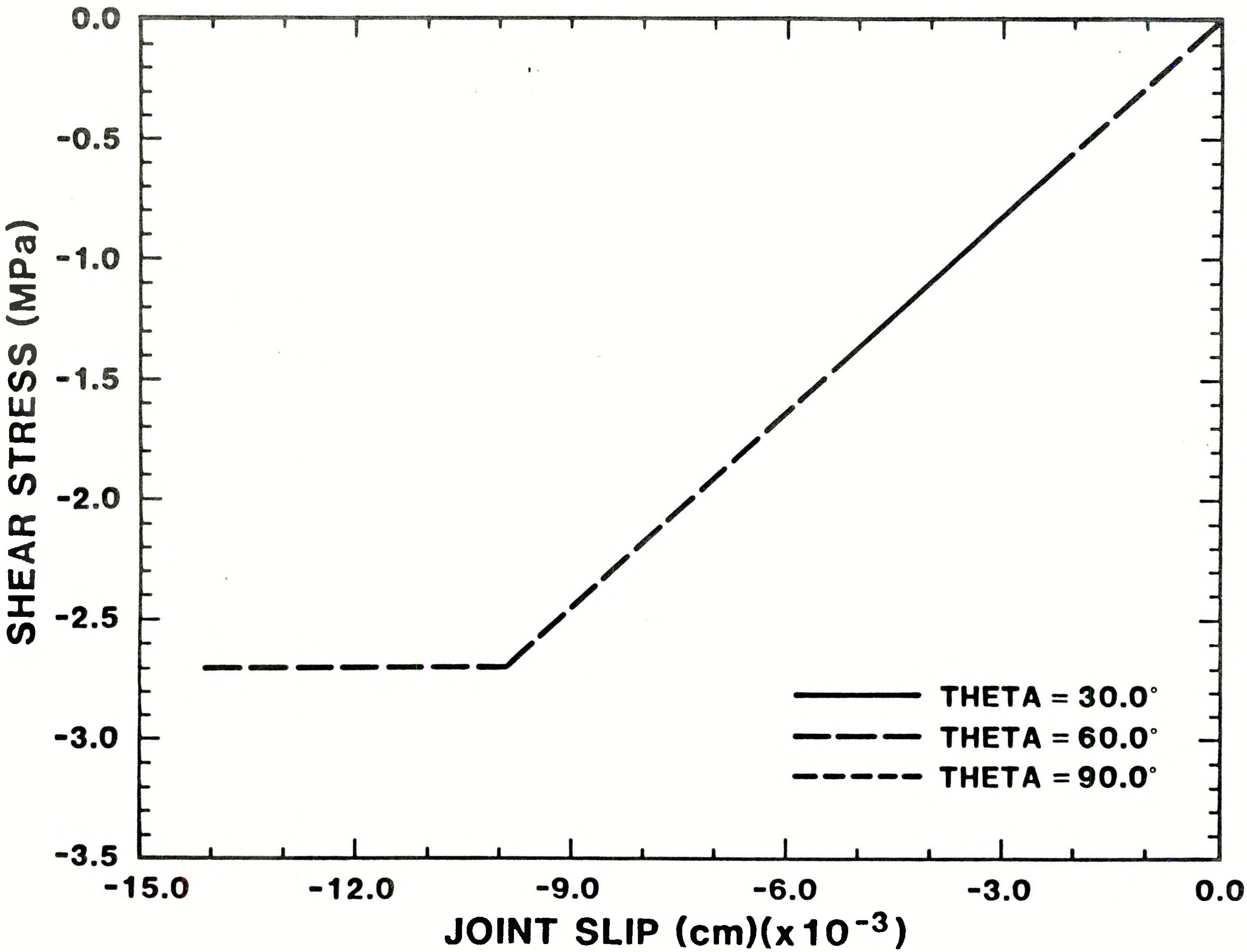

Figure 11. Stress-Slip Behavior for Joint Set 2, Example 2

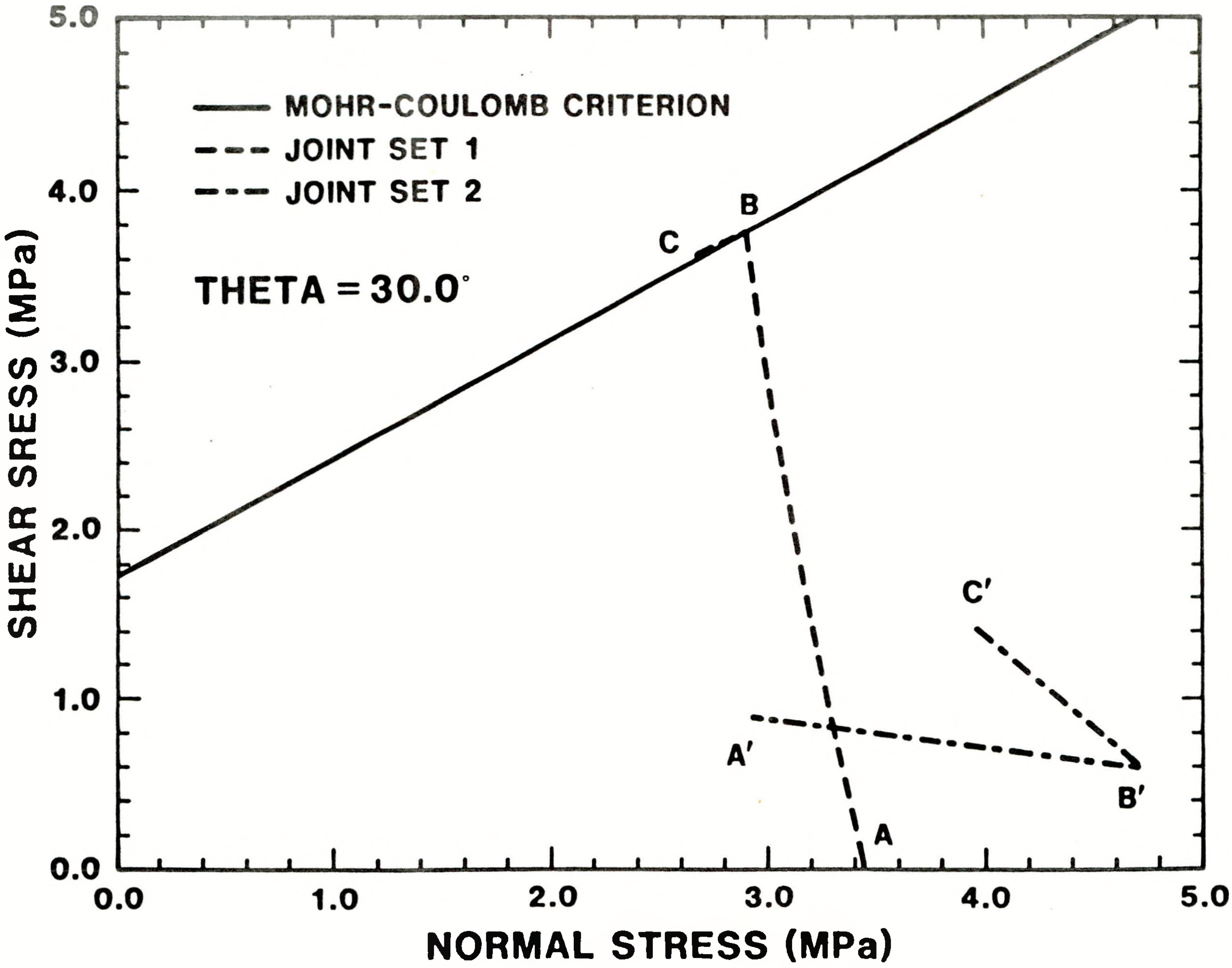

Figure 12. Load Path in Stress Space, θ = 30°

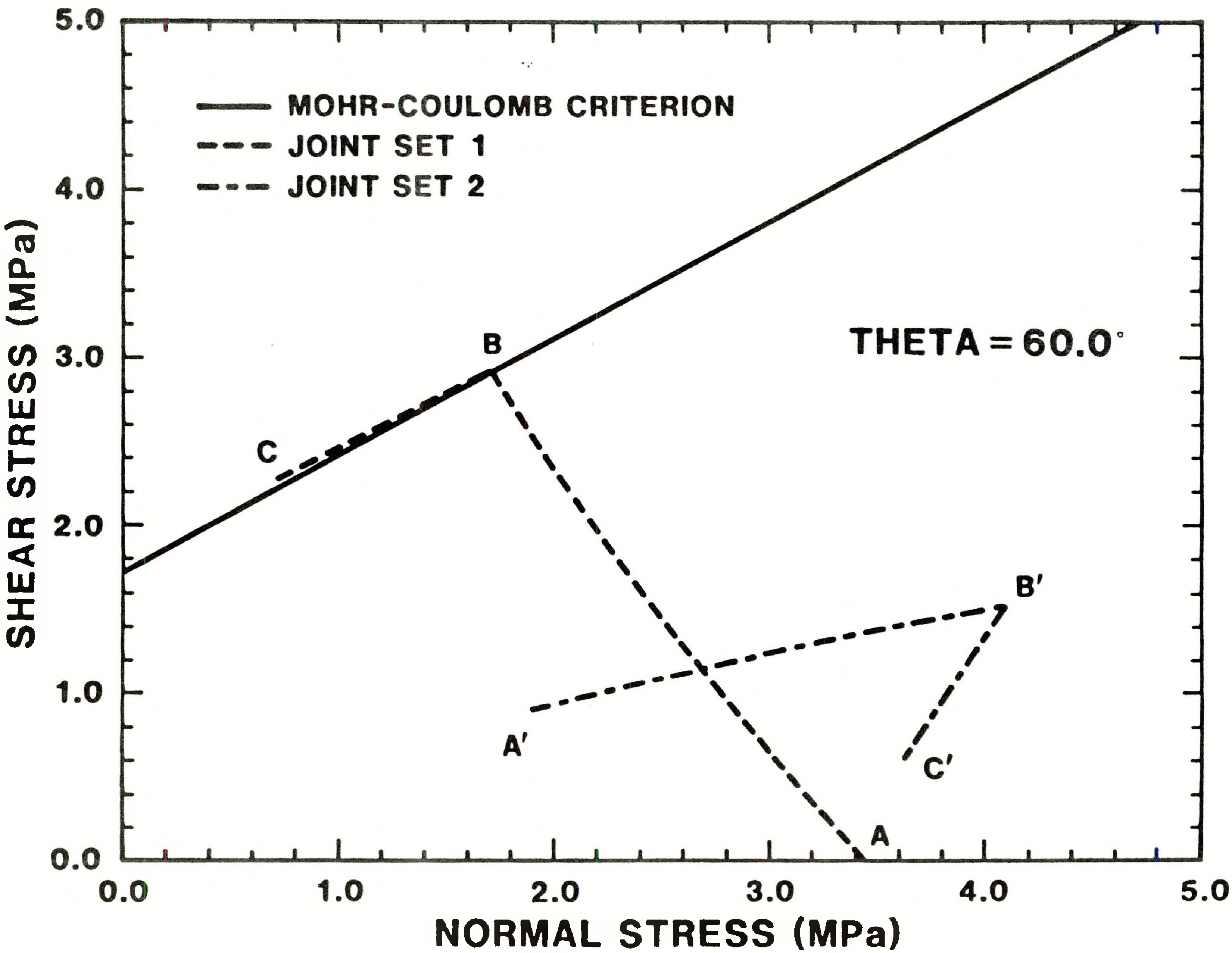

Figure 13. Load Path in Stress Space, θ = 60°

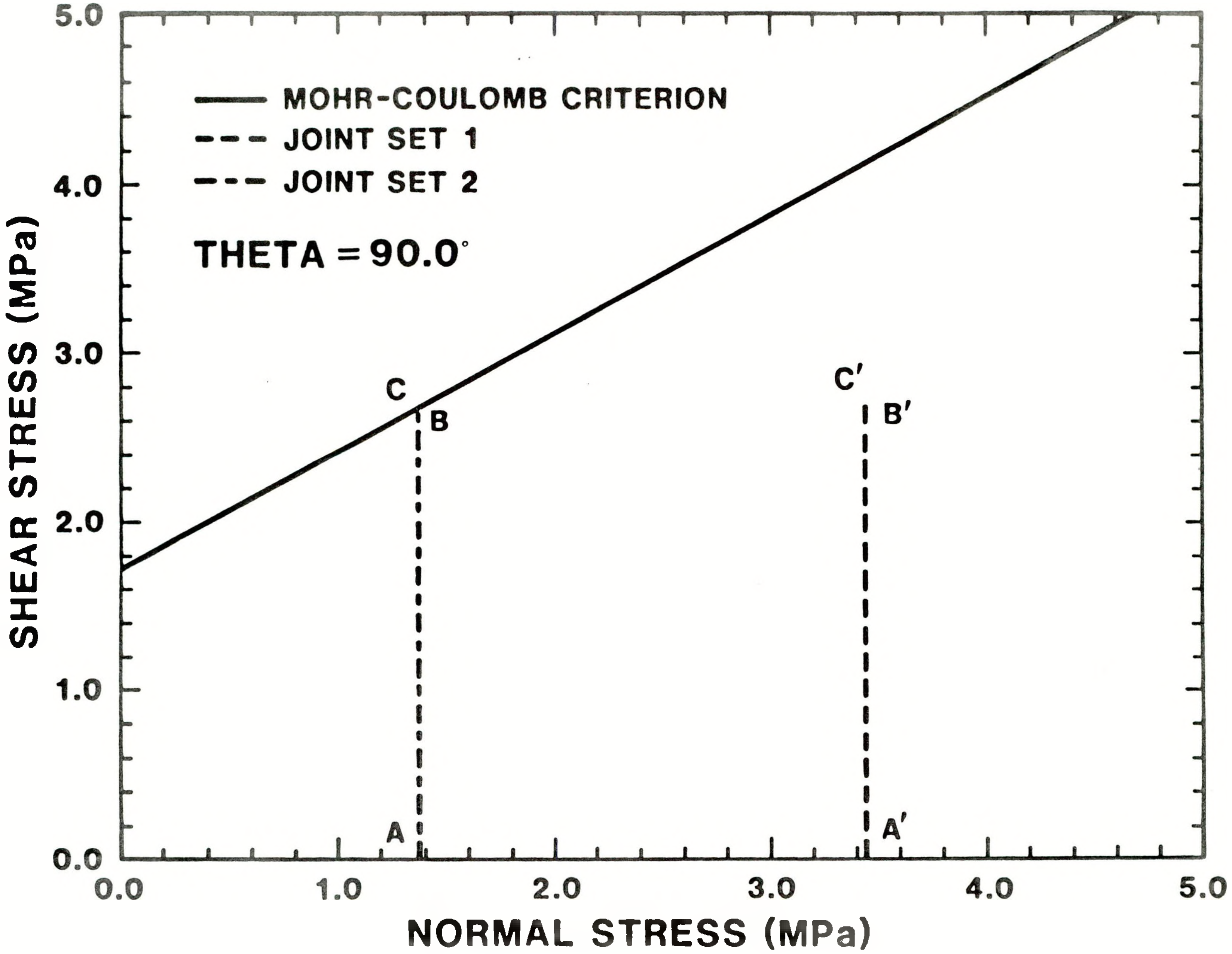

Figure 14. Load Path in Stress Space, θ = 90°

behavior for θ equals 60° is similar to that for θ equals 30° in which the first joint set has reached slip nonlinearity while the second joint set remains in the linear range. Because the joint sets are mutually orthogonal, the normal stresses on both joint sets do not change during the straining process for the θ equal 90° case. Because the second joint set has a lower normal stress, it reaches slip nonlinearity before the same can be accomplished by the first joint set. After the onset of slip nonlinearity (points B and B'), equilibrium dictates that shear stresses for the two joint sets must be equal. Therefore, throughout the shear straining process, joint set 1 remains in the linear range.

It is interesting to note from Figure 10 that beyond the points of initiation of slip nonlinearity, the shear stresses decrease with increasing joint-slip displacement. This is due to the effect of changing normal stresses. Although no normal strain is applied to the rock mass, the normal stress on the joint sets varies during the entire loading process because of the nonorthogonal joint orientation. As the magnitude of the normal stress decreases, the shear stress magnitude governing the onset of slip nonlinearity calculated from the Mohr-Coulomb criterion decreases. Hence, the softening of the shear stress-slip displacement curve is observed. For θ equal to 60°, this effect of the changing normal stress on the shear curve is shown in Figure 15.

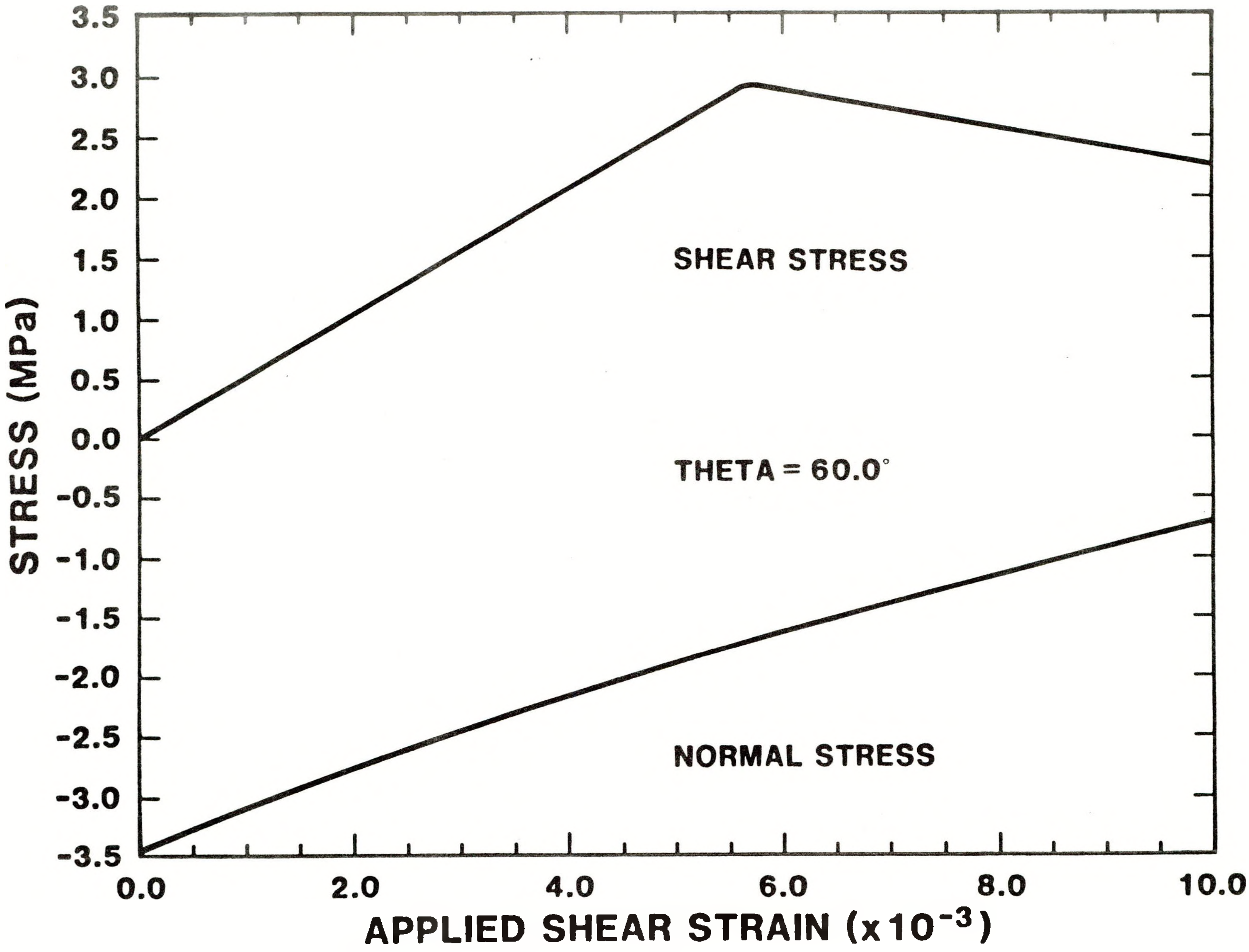

Figure 15. Stress-Strain Behavior for Joint Set 1, θ = 60°

4. Summary

A general constitutive model that describes the response of jointed rock mass with nonorthogonal sets of joints has been developed. Rate equations that govern the solution process have been presented, and a driver program for the constitutive model has been written and used to solve example problems. Results from these examples show complex interactions resulting from the nonorthogonal orientation of the joint sets.

5. References

Chen, E. P., 1986, Two-Dimensional Continuum Model for Jointed Media with Orthogonal Set of Joints, Proceedings of the 27th U. S. Symposium on Rock Mechanics, edited by H. L. Hartman, Society of Mining Engineers, Inc., Littleton, Colorado, pp. 862-867. (NNA.891109.0126)

Chen, E. P., 1989, A Constitutive Model for Jointed Rock Mass with Orthogonal Sets of Joints, Journal of Applied Mechanics, Vol. 56, pp. 25-32. (NNA.900319.0050)

Costin, L. S., and E. P. Chen, 1988a, An Analysis of the G-Tunnel Heated Block Experiment Using a Compliant-Joint Rock-Mass Model, Proceedings of the 29th U. S. Symposium on Rock Mechanics, edited by P. A. Cundall, R. L. Sterling, and A. M. Starfield, A. A. Balkema, Rotterdam, The Netherlands, pp. 625-632. (NNA.891013.0217)

Costin, L. S., and E. P. Chen, 1988b, An Analysis of the G-Tunnel Heated Block Thermomechanical Response Using a Compliant-Joint Rock-Mass Model, SAND87-2699, Sandia National Laboratories, Albuquerque, New Mexico. (NNA.881202.0210, HQS.880517.3048)

Goodman, R. E., 1976, Methods of Geological Engineering, pp. 300-368, West Publishing Company, St. Paul, Minnesota. (NNA.900502.0074)

Morland, L. W., 1974, Continuum Model of Regularly Jointed Medium, Journal of Geophysical Research, Vol. 79, No. 2, pp. 357-362. (NNA.890707.0061)

Thomas, R. K., 1982, Continuum Description for Jointed Media, SAND81-2615, Sandia National Laboratories, Albuquerque, New Mexico. (HQS.880517.1714)

Appendix

Information from the Reference Information Base Used in this Report

This report contains no information from the Reference Information Base.

Candidate Information for the Reference Information Base

This report contains no candidate information for the Reference Information Base.

Candidate Information for the Site and Engineering Properties Data Base

This report contains no candidate information for the Site and Engineering Properties Data Base.

DISTRIBUTION LIST

1 John W. Bartlett, Director (RW-1)
Office of Civilian Radioactive
Waste Management
U.S. Department of Energy
Forrestal Bldg.
Washington, D.C. 20585

1 F. G. Peters, Deputy Director (RW-2)
Office of Civilian Radioactive
Waste Management
U.S. Department of Energy
Forrestal Bldg.
Washington, D.C. 20585

1 Ralph Stein (RW-30)
Office of Civilian Radioactive
Waste Management
U.S. Department of Energy
Forrestal Bldg.
Washington, D.C. 20585

1 M. W. Frei (RW-22)
Office of Civilian Radioactive
Waste Management
U.S. Department of Energy
Forrestal Bldg.
Washington, D.C. 20585

1 B. G. Gale (RW-23)
Office of Civilian Radioactive
Waste Management
U.S. Department of Energy
Forrestal Bldg.
Washington, D.C. 20585

1 J. D. Saltzman (RW-5)
Office of External Relations
Office of Civilian Radioactive
Waste Management
U.S. Department of Energy
Forrestal Bldg.
Washington, D.C. 20585

1 S. J. Brocoum (RW-20)
Office of Civilian Radioactive
Waste Management
U.S. Department of Energy
Forrestal Building
Washington, D.C. 20585

1 T. H. Isaacs (RW-4)
Office of Stratigic Planning
and International Programs
Office of Civilian Radioactive
Waste Management
U.S. Department of Energy
Forrestal Bldg.
Washington, D.C. 20585

1 D. H. Alexander (RW-332)
Office of Civilian Radioactive
Waste Management
U.S. Department of Energy
Forrestal Bldg.
Washington, D.C. 20585

1 J. C. Bresee (RW-10)
Office of Civilian Radioactive
Waste Management
U.S. Department of Energy
Forrestal Bldg.
Washington, D.C. 20585

1 Samuel Rousso (RW-10)
Office of Program and Resources
Management
Office of Civilian Radioactive
Waste Management
U.S. Department of Energy
Forrestal Bldg.
Washington, D.C. 20585

1 Gerald Parker (RW-3[illegible])
Office of Civilian Radioactive
Waste Management
U.S. Department of Energy
Forrestal Bldg.
Washington, D.C. 20585

1 D. G. Horton (RW-3)
Office of Quality Assurance
Office of Civilian Radioactive
Waste Management
U.S. Department of Energy
Forrestal Bldg.
Washington, D.C. 20585

February 7, 1991

1 Robert E. Cummings
Engineers International, Inc.
P.O. Box 43817
Tucson, AZ 85733-3817

1 Dr. Jaak J. K. Daemen
University of Nevada
Mackay School of Mines
Reno, NV 89557-0139

1 Department of Comprehensive Planning
Clark County
225 Bridger Avenue, 7th Floor
Las Vegas, NV 89155

1 Economic Development Department
City of Las Vegas
400 East Stewart Avenue
Las Vegas, NV 89109

1 Planning Department
Nye County
P.O. Box 153
Tonopah, NV 89049

1 Director of Community Planning
City of Boulder City
P.O. Box 367
Boulder City, NV 89005

1 Commission of the European
Communities
200 Rue de la Loi
B-1049 Brussels
Belgium

1 Lincoln County Commission
Lincoln County
P.O. Box 90
Pioche, NV 89043

1 Community Planning & Development
City of North Las Vegas
P.O. Box 4086
North Las Vegas, NV 89030

1 City Manager
City of Henderson
Henderson, NV 89015

1 ONWI Library
Battelle Columbus Laboratory
Office of Nuclear Waste Isolation
505 King Avenue
Columbus, OH 43201

1 Librarian
Los Alamos Technical
Associates, Inc.
P.O. Box 410
Los Alamos, NM 87544

1 Loren Lorig
Itasca Consulting Group, Inc.
1313 5th Street SE, Suite 210
Minneapolis, MN 55414

1 James K. Lein
Department of Geography
122 Clippinger Laboratories
Ohio University
Athens, OH 45701-2979

1	6300	T. O. Hunter, Actg.
1	6310	T. E. Blejwas, Actg.
1	6310A	F. W. Bingham
1	6310	YMP CRF
1	6310	100/124231/SAND89-0592/QA
1	6311	A. L. Stevens
1	6312	F. W. Bingham, Actg.
1	6313	L. E. Shephard, Actg.
1	6314	L. S. Costin
1	6314	S. J. Bauer
1	6315	F. B. Nimick, Actg.
1	6316	R. P. Sandoval
1	6317	S. Sinnock
2	6318	L. J. Erickson
1	6318	C. Crawford for Accession No. Data Base
1	6319	R. R. Richards
20	6341	WMT Library
1	6410	D. J. McCloskey, Actg.
5	3141	S. A. Landenberger
3	3151	G. L. Esch
1	8524	J. A. Wackerly
8	3145	Document Processing for DOE/OSTI
1	1425	J. Jung
1	1510	J. C. Cummings
10	1514	E. P. Chen
1	1514	J. F. Holland
1	1514	R. L. Johnson
1	1514	J. R. Koteras
1	1514	H. S. Morgan

1 D. E. Shelor (RW-30)
Office of Systems and Compliance
Office of Civilian Radioactive
Waste Management
U.S. Department of Energy
Forrestal Bldg.
Washington, D.C. 20585

1 L. H. Barrett (RW-40)
Office of Storage and Transportation
Office of Civilian Radioactive
Waste Management
U.S. Department of Energy
Forrestal Bldg.
Washington, D.C. 20585

1 F. G. Peters (RW-50)
Office of Contractor Business
Management
Office of Civilian Radioactive
Waste Management
U.S. Department of Energy
Forrestal Bldg.
Washington, D.C. 20585

1 Senior Project Manager for Yucca
Mountain Repository Project Branch
Division of Waste Management
U.S. Nuclear Regulatory Commission
Washington, D.C. 20555

1 NTS Section Leader
Repository Project Branch
Division of Waste Management
U.S. Nuclear Regulatory Commission
Washington, D.C. 20555

1 Repository Licensing & Quality
Assurance Project Directorate
Division of Waste Management
U.S. Nuclear Regulatory Commission
Washington, DC 20555

1 NRC Document Control Clerk
Division of Waste Management
U.S. Nuclear Regulatory Commission
Washington, D.C. 20555

1 Carl P. Gertz (RW-20)
Office of Geologic Disposal
Office of Civilian Radioactive
Waste Management
U.S. Department of Energy
Forrestal Bldg.
Washington, D.C. 20585

1 D. U. Deere, Chairman
Nuclear Waste Technical
Review Board
1100 Wilson Blvd. #910
Arlington, VA 22209-2297

1 NRC Document Control Desk
Division of Waste Management
U.S. Nuclear Regulatory Commission
Washington, D.C. 20555

5 Carl P. Gertz, Project Manager
Yucca Mountain Project Office
Nevada Operations Office
U.S. Department of Energy
Mail Stop 523
P.O. Box 98518
Las Vegas, NV 89193-8518

12 Technical Information Office
Nevada Operations Office
U. S. Department of Energy
P.O. Box 98518
Las Vegas, NV 89193-8518

1 [illegible] West, Director
Office of External Affairs
Nevada Operations Office
U.S. Department of Energy
P.O. Box 98518
Las Vegas, NV 89193-8518

1 W. M. Hewitt, Program Manager
Roy F. Weston, Inc.
955 L'Enfant Plaza, Southwest
Suite 800
Washington, D.C. 20024

1 Technical Information Center
Roy F. Weston, Inc.
955 L'Enfant Plaza, Southwest
Suite 800
Washington, D.C. 20024

3 L. J. Jardine
Technical Project Officer for YMP
Lawrence Livermore National Laboratory
Mail Stop L-204
P.O. Box 808
Livermore, CA 94550

1 J. H. Nelson
Technical Project Officer for YMP
Science Applications International Corp.
101 Convention Center Dr.
Suite 407
Las Vegas, NV 89109

1 H. N. Kalia
Exploratory Shaft Test Manager
Los Alamos National Laboratory
Mail Stop 527
101 Convention Center Dr.
Suite 820
Las Vegas, NV 89109

1 Arend Meijer
Los Alamos National Laboratory
Mail Stop J514
P.O. Box 1663
Los Alamos, NM 87545

4 R. J. Herbst
Technical Project Officer for YMP
Los Alamos National Laboratory
N-5, Mail Stop J521
P.O. Box 1663
Los Alamos, NM 87545

6 L. R. Hayes
Technical Project Officer for YMP
U.S. Geological Survey
P.O. Box 25046
421 Federal Center
Denver, CO 80225

1 K. W. Causseaux
NHP Reports Chief
U.S. Geological Survey
P.O. Box 25046
421 Federal Center
Denver, CO 80225

1 R. V. Watkins, Chief
Project Planning and Management
U.S. Geological Survey
P.O. Box 25046
421 Federal Center
Denver, CO 80225

1 Center for Nuclear Waste Regulatory Analyses
6220 Culebra Road
Drawer 28510
San Antonio, TX 78284

1 D. L. Lockwood, General Manager
Raytheon Services, Inc.
Mail Stop 514
P.O. Box 93265
Las Vegas, NV 89193-3265

1 Richard L. Bullock
Technical Project Officer for YMP
Raytheon Services, Inc.
101 Convention Center Dr.
Suite P250
Las Vegas, NV 89109

1 James C. Calovini
Raytheon Services, Inc.
101 Convention Center Dr.
Suite P-280
Las Vegas, NV 89109

1 Dr. David W. Harris
YMP Technical Project Officer
Bureau of Reclamation
P.O. Box 25007 Bldg. 67
Denver Federal Center
Denver, CO 80225-0007

1 A. E. Gurrola
General Manager
Raytheon, Inc.
Mail Stop 580
P.O. Box 93838
Las Vegas, NV 89193-3838

1 M. D. Voegele
Science Applications International Corp.
101 Convention Center Dr.
Suite 407
Las Vegas, NV 89109

1 P. T. Prestholt
NRC Site Representative
1050 East Flamingo Road
Suite 319
Las Vegas, NV 89119

1 R. E. Lowder
Technical Project Officer for YMP
MAC Technical Services
Valley Bank Center
101 Convention Center Drive
Suite 1100
Las Vegas, NV 89109

1 D. L. Fraser, General Manager
Reynolds Electrical & Engineering Co.
P.O. Box 98521
Mail Stop 555
Las Vegas, NV 89193-8521

1 P. K. Fitzsimmons, Director
Health Physics & Environmental Division
Nevada Operations Office
U.S. Department of Energy
P.O. Box 98518
Las Vegas, NV 89193-8518

1 Robert F. Pritchett
Technical Project Officer for YMP
Reynolds Electrical & Engineering Co.
Mail Stop 615
P.O. Box 98521
Las Vegas, NV 89193-8521

1 D. Zesiger
U.S. Geological Survey
101 Convention Center Dr.
Suite 860 - MS509
Las Vegas, NV 89109

1 Elaine Ezra
YMP GIS Project Manager
EG&G Energy Measurements, Inc.
P.O. Box 1912
Mail Stop H-02
Las Vegas, NV 89125

2 SAIC-T&MSS Library
Science Applications International Corp.
101 Convention Center Dr.
Suite 407
Las Vegas, NV 89109

1 Dr. Martin Mifflin
Desert Research Institute
Water Resources Center
2505 Chandler Avenue
Suite 1
Las Vegas, NV 89120

1 E. P. Binnall
Field Systems Group Leader
Building 50B/4235
Lawrence Berkeley Laboratory
Berkeley, CA 94720

1 J. F. Divine
Assistant Director for Engineering Geology
U.S. Geological Survey
106 National Center
12201 Sunrise Valley Dr.
Reston, VA 22092

1 V. M. Glanzman
U.S. Geological Survey
P.O. Box 25046
913 Federal Center
Denver, CO 80225

1 C. H. Johnson
Technical Program Manager
Nuclear Waste Project Office
State of Nevada
Evergreen Center, Suite 252
1802 North Carson Street
Carson City, NV 89710

1 T. Hay, Executive Assistant
Office of the Governor
State of Nevada
Capitol Complex
Carson City, NV 89710

3 R. R. Loux, Jr.
Executive Director
Nuclear Waste Project Office
State of Nevada
Evergreen Center, Suite 252
1802 North Carson Street
Carson City, NV 89710

1 John Fordham
Water Resources Center
Desert Research Institute
P.O. Box 60220
Reno, NV 89506

1 Prof. S. W. Dickson
Department of Geological Sciences
Mackay School of Mines
University of Nevada
Reno, NV 89557

1 J. R. Rollo
Deputy Assistant Director for
Engineering Geology
U.S. Geological Survey
106 National Center
12201 Sunrise Valley Dr.
Reston, VA 22092

1 Eric Anderson
Mountain West Research-Southwest
Inc.
2901 N. Central Ave. #1000
Phoenix, AZ 85012-2730

5 Judy Foremaster
City of Caliente
P.O. Box 158
Caliente, NV 89008

1 D. J. Bales
Science and Technology Division
Office of Scientific and Technical
Information
U.S. Department of Energy
P.O. Box 62
Oak Ridge, TN 37831

1 Carlos G. Bell, Jr.
Professor of Civil Engineering
Civil and Mechanical Engineering
Department
University of Nevada, Las Vegas
4505 South Maryland Parkway
Las Vegas, NV 89154

1 C. F. Costa, Director
Nuclear Radiation Assessment
Division
U.S. Environmental Protection
Agency
Environmental Monitoring Systems
Laboratory
P.O. Box 93478
Las Vegas, NV 89193-3478

1 J. Z. Bem
Project Manager
Bechtel National Inc.
P.O. Box 3965
San Francisco, CA 94119

1 R. Harig
Parsons Brinckerhoff Quade &
Douglas
303 Second Street
Suite 700 North
San Francisco, CA 94107-1317

1 Dr. Roger Kasperson
CENTED
Clark University
950 Main Street
Worcester, MA 01610

The number in the lower right-hand corner is an accession number used for Office of Civilian Radioactive Waste Management purposes only. It should not be used when ordering this publication.

Org.	Bldg.	Name	Rec'd by	Org.	Bldg.	Name	Rec'd by

Sandia National Laboratories